Fundamental properties of Ca^{2+} signals

Kevin Thurley[a], Alexander Skupin[b], Rüdiger Thul[c], Martin Falcke[a,d]

[a] Max Delbrück Centre for Molecular Medicine, Robert-Rössle-Str. 10, 13125 Berlin, Germany, kevin.thurley@mdc-berlin.de, martin.falcke@mdc-berlin.de

[b] Luxembourg Centre of Systems Biomedicine, 162a, avenue de la Faiencerie, L-1511 Luxembourg, and Institute for Systems Biology, 401 Terry Avenue North, Seattle, WA 98103-8904, USA, alexander.skupin@uni.lu

[c] School of Mathematical Sciences, University of Nottingham, Nottingham, NG7 2RD, UK, ruediger.thul@nottingham.ac.uk

[d] corresponding author

Ca^{2+} is a ubiquitous and versatile second messenger that primarily transmits information through rises and falls of the cytosolic Ca^{2+} concentration. After reviewing recent findings on key characteristics of the cytosolic Ca^{2+} dynamics, we demonstrate the importance of the hierarchal arrangement of Ca^{2+} release sites on the emergence of cellular Ca^{2+} spikes and present theoretical concepts that explain the wide range of experimentally observed Ca^{2+} signals. We relate properties of the dynamical regulation of the cytosolic Ca^{2+} concentration to ideas about information transmission by Ca^{2+} spike sequences. Our findings highlight that stochastic Ca^{2+} signals are functionally robust and adaptive to changing environmental conditions.

Keywords: calcium dynamics, mathematical modeling, cell signaling, stochastic processes

Highlights: > We review recent findings on key characteristics of cytosolic Ca^{2+} dynamics. > We demonstrate the importance of the hierarchal arrangement of Ca^{2+} release sites. > New theoretical concepts exploit emergent behavior of cellular Ca^{2+} spikes. > We relate the dynamical regulation of $[Ca^{2+}]$ to information transmission. > Stochastic Ca^{2+} signals are functionally robust and adaptive to changing conditions.

1. Introduction

The Ca^{2+} signaling pathway translates external signals into intracellular responses by increasing the cytosolic Ca^{2+} concentration in a stimulus dependent pattern. The concentration increase can be caused either by Ca^{2+} entry from the extracellular medium through plasma membrane channels, or by Ca^{2+} release from internal storage compartments. In the following, we will focus on inositol 1,4,5-trisphosphate (IP_3)-induced Ca^{2+} release from the endoplasmic reticulum (ER), which is the predominant Ca^{2+} release mechanism in many cell types. The signal cascade starts typically at a plasma membrane G-protein coupled receptor [1-3]. Due to binding of an agonist, the receptor activates phospholipase C (PLC), which in turn produces IP_3 at the cell membrane. IP_3 diffuses in the cytosol and binds to IP_3 receptor channels (IP_3Rs), where subsequent binding of Ca^{2+} to activating Ca^{2+} binding sites switches the channel to a state with high open probability [4]. This positive feedback of Ca^{2+} on its own release channel is called Ca^{2+}-induced-Ca^{2+}-release (CICR). Opening of an IP_3R triggers a Ca^{2+} flux into the cytosol due to the large concentration differences between the two compartments [4-7], which is in the range of 3 to 4 orders of magnitudes. The released Ca^{2+} is removed from the cytosol either by sarco-endoplasmic reticulum Ca^{2+} ATPases (SERCAs) into the ER or by plasma membrane Ca^{2+} ATPases into the extracellular space.

IP_3R are spatially organized into clusters of up to about fifteen channels, which are scattered across the ER membrane with distances of 1 to 7 μm [8-12]. The coupling between channels is achieved through CICR based on Ca^{2+} diffusion. Given that the diffusion length of Ca^{2+} is less than 2 μm, the coupling between channels in a cluster is much stronger than the coupling between channels in adjacent clusters [13]. The structural hierarchy of IP_3R from the single channel to clusters is also reflected in the dynamic responses of the intracellular Ca^{2+} concentration as revealed through fluorescence microscopy and simulations [12, 14-17]. Openings of single IP_3Rs ('blips') may trigger collective openings of IP_3Rs within a cluster ('puffs'), while Ca^{2+} diffusing from a puff site can then activate neighboring clusters, eventually leading to a global, i.e. cell wide, Ca^{2+} spike [15]. Marchant and Parker followed the signal generation from its origin at a single channel cluster to the global Ca^{2+} wave, which corresponds to a concentration spike in whole cell recordings [15, 18]. Importantly, repetitive sequences of these Ca^{2+} spikes encode information that is used to regulate many processes in various cell types [19-21].

Cellular spike sequences exhibit a refractory period after a spike [22-26]. The refractoriness has often been related to the negative feedback of high Ca^{2+} concentrations on the open probability of IP_3R as observed in patch clamp experiments [27-29] (see [5, 30, 31] for reviews). Together with the positive feedback of CICR at small Ca^{2+} concentrations, this negative feedback leads to a bell shaped dependence of the stationary open probability of IP_3R on cytosolic Ca^{2+} [6, 32]. The negative feedback causes an almost fixed (or deterministic) refractory period of several tens of seconds in the global signals. However, such a recovery timescale has not been observed with the local puff dynamics of IP_3R clusters. Interpuff intervals (IPIs) exhibit a relative refractory period of a few seconds only [12, 14, 15, 18, 33-35]. Hence, the negative feedback that determines the time scale of interspike intervals (ISIs) is different from the feedback contributing to IPI and requires global (whole cell) release events.

Here, we review the dynamic properties of Ca^{2+} spike sequences. An important property of ISIs (and IPIs) is that they form a distribution. Rather than having a single value for the ISI, cells exhibit a spread of times between consecutive spikes. The very existence of a distribution of ISIs hints at the presence of fluctuations somewhere in the spike generation process. Broadly speaking, these fluctuations can

arise from two different types of processes. With the first one, the variations arise from deviations around a constant ISI. In this context, we would assume that the fundamental process giving rise to the constant ISI is a deterministic oscillator. With the second one, the emergence of each spike is completely random. In this case, the dynamics are truly stochastic. The first process would generate regular spike sequences without fluctuations, the second process would not generate any spikes without fluctuations. The distinction between a deterministic and a stochastic spike generation mechanism is not only important for the choice of the appropriate mathematical description, but also points towards the fundamental biological processes that are involved in shaping ISIs.

To test the two approaches, we take advantage of the fact that they make different predictions with respect to the dependence of spike characteristics on cellular parameters. For example, stochastic models reproduce the sensitive dependence of the average ISI on the diffusional properties of the cytosol, while deterministic models predict independence of the average ISI from diffusion coefficients and buffer concentrations [26, 36]. Similar considerations apply to other correlations [16, 26, 37, 38]. Stochastic models reconcile dissociation constants of the Ca^{2+} regulatory binding sites on the IP_3R measured *in vitro* with the dynamic behavior and local concentrations *in vivo* [17], and they offer straightforward explanations for the large measured cell-to-cell variability of the average ISI [36, 39]. Moreover, the standard deviation of ISIs within a single spike sequence is in many cases of the same order of magnitude as the average value, and these fluctuations are an additional source of information. As we will see below, the standard deviation presents a better indicator for the IP_3R open probability than the average ISI. The former is governed by the randomness of the spike generation mechanism, while the latter is mostly determined by a global feedback.

Deterministic models have contributed substantially to the development of concepts and ideas in the field. One of the first theoretical considerations was undertaken by Meyer and Stryer in 1988 [40], who used a nonlinear dependence of the release flux on the IP_3 concentration and suggested a feedback through IP_3 oscillations. This hypothesized feedback could not be verified experimentally in general and led to further model development. A prominent class of models for the IP_3 receptor (see [5, 30, 31, 41] for reviews) considers one site for IP_3 binding that sensitizes a subunit for Ca^{2+} binding, one for Ca^{2+} that activates a subunit, and another one for Ca^{2+} that dominantly inhibits a subunit. In the DeYoung-Keizer-model [27], it is assumed that a channel opens if at least 3 subunits of the tetrameric IP_3R are in the active state. The different affinities for Ca^{2+} binding to the activating and inhibiting binding sites lead to a bell shaped stationary open probability of an IP_3R [5, 32]. Another conceptually important model was introduced by Goldbeter et al. [42, 43]. It is based on the existence of two Ca^{2+} pools representing the ER and the cytosol, respectively. Increasing IP_3 triggers Ca^{2+} release from the ER into the cytosol inducing further CICR by a positive feedback. After emptying the ER, Ca^{2+} is pumped back by SERCAs into the ER. Repeating this scenario leads to oscillations with similar properties as those observed in experiments.

With the improvement of experimental techniques, a growing number of measurements were published that could not be explained within the framework of deterministic models, which neglected the spatial arrangement of IP_3R clusters. More precisely, these models did not incorporate the Ca^{2+} concentration gradients around an open IP_3R cluster and the weaker diffusive coupling between clusters, as compared to within clusters (see below). Furthermore, the averaging procedure that leads from the mathematical description of all the individual channels in a cell (master equation) to the rate equations of deterministic models identifies *small* probabilities with *small* currents. If the cell is in a state with small open probability, a small fraction of channels is open and causes a small release flux. On the contrary, stochastic models that take channel clustering into account identify small probabilities with *rare* events that cause locally large concentration changes and have the potential to cause initiate global spikes [16, 36, 39]. We will see below that this hierarchic cascade of events (Figure 1) gives rise to dynamical

properties and parameter dependences different from those in deterministic models.

2. The dynamics of IP_3R clusters

The local Ca^{2+} concentration at open channels is orders of magnitude larger than the spatially averaged bulk concentrations [44]. Single open channels may cause Ca^{2+} concentrations in a volume of the size of the IP_3R channel vestibule of 20-70 μM, several open channels of up to 220 μM [13]. The concentration at a distance of only 1 μm from the cluster is orders of magnitude smaller.

These large Ca^{2+} gradients around an open cluster of IP_3R also raised the question whether the nonlinear interplay between Ca^{2+} release and Ca^{2+} uptake suffices to reproduce the Ca^{2+} spike sequences observed in experiments. To answer this question, we studied a deterministic model of a single cluster in a three dimensional cytosolic environment [17]. The flux through a Ca^{2+} liberating cluster was chosen according to realistic simulations [13] and determined by the number of open channels. To compute this number, we employed the DeYoung Keizer model as a prototypical framework for IP_3R dynamics [45]. Based on Ca^{2+} fluxes that lead to realistic Ca^{2+} concentrations at a releasing cluster [13], the deterministic cluster model does not generate oscillations. After an initial release phase, all channels within the cluster close and remain inactive forever.

We may understand this behavior by considering the impact of the large Ca^{2+} concentrations on the nonlinear feedback functions that regulate Ca^{2+} liberation. Assuming that these functions are of Hill type (as is the case in most IP_3R models), a good measure of the dynamic range of the feedback is the dissociation constant K_D. Generally speaking, feedback only exists if the Ca^{2+} concentration is in the range of the dissociation constant. For Ca^{2+} activation, the dissociation constant is in the order of 100-500 nM, while Ca^{2+} inhibition is governed by a K_D of around 2 μM [46, 47]. Keeping in mind that Ca^{2+} concentrations at a releasing cluster reach peak values of 20-220μM [13], all feedback processes saturate. Almost all channels in a cluster become inhibited, they remain inactive even when the Ca^{2+} concentration drops an order of magnitude. A concentration keeping most channels inhibited can be maintained with a tiny fraction of channels that remain active. Although inhibition is removed at basal concentration values, the Ca^{2+} concentration is now below the dynamic range of Ca^{2+} activation, locking the cluster in the closed state.

Given that the existence of deterministic oscillations depend on whether feedback processes saturated or not, we investigated the dynamic regimes of the model in more detail [48]. Indeed, the deterministic cluster model supports oscillations. However, these are not the oscillations seen in experiments. Firstly, the oscillatory regime with respect to the IP_3 concentration is too small to be accessed in any measurement. Secondly, the oscillation amplitude is too small. At a distance of 1.6μm from the cluster center, the Ca^{2+} concentration oscillates in the nM range with amplitudes of less than 1nM [17]. These oscillations could never be observed, nor would they be strong enough to activate adjacent clusters. It is worth pointing out that there are multiple potential mechanisms that underlie the disappearance of the oscillations including a significant increase in the period (homoclinic bifurcation) and potential chaotic behavior (period doubling cascade).

To reinstate oscillations at a single cluster, we have to incorporate discrete, integer channel numbers in clusters and fluctuations at the single channel level. The random opening of a channel prevents it from locking in the closed state, and closing of the last channel spontaneously or due to inhibition prevents the tiny fraction of open channels from maintaining inhibiting concentrations. Importantly, these fluctuations are not due to a small number of Ca^{2+} ions near a channel. The noise stems from the small number of subunits of a channel with only a few binding sites each, since stochastic binding of a few IP_3 molecules and Ca^{2+} ions leads to significant state changes. This discreteness forecloses smearing out fluctuations by the law of large numbers, and it violates the identification of small probabilities

with small fluxes mentioned above.

This theoretical study has recently been confirmed by experimental results. We investigated in detail the IPI distributions in SH-SY5Y cells and HEK 293 cells [35]. IPI distributions reveal a relative refractory period of a few seconds on the cluster level, which is in good agreement with earlier studies [12, 14, 33, 49]. The average IPI is typically one order of magnitude shorter than the average ISI. Our analysis does not reveal any indication of periodicity, neither on the time scale of IPIs nor on the time scale of ISIs across puff sequences. Therefore, theoretical and experimental studies have demonstrated the lack of the time scale of cellular signals in the cluster dynamics.

The probability λ for a puff can be fitted by an ansatz assuming recovery from negative feedback with a rate ξ and an asymptotic probability λ_0 [35]:

$$\lambda(t) = \lambda_0(1 - e^{-\xi t}),$$

leading to the IPI distribution p

$$p(t) = \lambda_0(1 - e^{-\xi t}) \exp[-\int_0^t \lambda_0(1 - e^{-\xi t'})dt'] = \lambda_0(1 - e^{-\xi t})e^{-\lambda_0 t} \exp\left[\frac{\lambda_0}{\xi}\left(1 - e^{-\xi t}\right)\right] \quad (1)$$

The variable t denotes the time passed since the last puff. Individual puff sites of a same cell exhibit large heterogeneity with respect to the values of ξ and λ_0. Values for λ_0 are in the range from 0.18 s^{-1} to 0.5 s^{-1} for SH-SY5Y cells and from 0.5 s^{-1} to 3 s^{-1} in HEK 293 cells, and values for ξ from 0.4 s^{-1} to 4 s^{-1} for SH-SY5Y cells and from 1 s^{-1} to 90 s^{-1} in HEK 293 cells. Distributions with large values of ξ can also be fitted simply by the exponential distribution, $p(t)=\lambda_0 \exp(-\lambda_0 t)$. Clearly, the recovery from negative feedback distinguishes both cell types.

The above distribution and the IPI histograms exhibit only one maximum but no higher order maxima at integer multiples of a period. Hence, they do not support the assumption of periodicity on the time scale of an average IPI. We could not find any evidence for periodicity, neither on the time scale of several IPIs nor on the time scale of cellular ISIs [35].

Smith et al. found that the number of open channels during a puff rapidly reaches a maximum value. Afterwards, they close randomly and independently with an average rate γ=1/(0.017 s) [50]. These results imply a puff duration distribution d which obeys

$$d(t) = N\gamma e^{-\gamma t}\left(1 - e^{-\gamma t}\right)^{N-1}, \quad (2)$$

with t denoting the duration of the puff and N denoting the number of channels that are open at the peak of the puff. N varies from puff to puff, indicating that not all of the available channels within a cluster participate in every puff. Once the first channel opens, the recruitment of additional channels follows a probability that is proportional to the third root of already open channels [50]. This could, to a large part, be due to the dependence of the local Ca^{2+} concentration on the number of open channels [13, 51]. Puff amplitudes show weak or no correlation with the amplitude of the preceding puff or the preceding IPI [8, 35, 50, 52]. Hence, this less than maximal response to the opening of the first channel in the cluster cannot be explained by incomplete recovery from a negative feedback.

In summary, channel clusters have typical dynamics different from both the behavior of isolated channels in patch clamp experiments with clamped concentrations as well as cellular dynamics. The cluster dynamics are random with time scales a few times faster than cellular spiking.

3. The dynamics of cellular Ca^{2+} spike sequences and the origin of robustness

How does the cellular time scale emerge from puff dynamics? The generation of a cellular concentration spike has been observed in detail in *Xenopus* oocytes [15, 18]. Not every puff causes a global spike but several channel clusters have to open in synchrony in order to activate all other IP_3R clusters. Ca^{2+} diffusing from the puff site opening first may activate neighboring clusters, but a sufficient number of puffs for setting off a global spike is reached only with some probability (coupling probability), not with certainty. The smaller this probability is, the more attempts are required to cause a global spike and the larger is the ratio ISI/IPI. The initiation of such a wave (of Ca^{2+} release) from an initial event is called wave nucleation. The minimal number of open clusters causing a global spike with almost certainty is called the critical nucleus. The coupling probability depends sensitively on the strength of the spatial coupling – and so does the average length of the ISIs. The diffusion of free Ca^{2+} can be easily reduced by loading Ca^{2+}-buffers into the cytosol. Indeed, the average ISI and the standard deviation (SD) of ISIs depend sensitively on the buffer concentration, also in cells much smaller than the *Xenopus* oocyte (e.g. HEK and PLA cells, astrocytes, microglia) [26].

The observation that average and standard deviation of ISIs increase in a coordinated fashion shows that the same process determines average length and fluctuations. We conclude that the wave nucleation mechanism applies also to small cells, which is additionally corroborated by the observation of preferred spike initiation centers in some cells [53]. Figure 2 shows typical data. The relation between the SD and the average ISI (moment relation) reveals the existence of a minimal interspike interval, which is observed at high stimulation [26]. The minimal ISI indicates the time that cells need to recover from the previous spike. At high stimulation, the probability for nucleation of a wave is very high, and the next spike comes up very soon after recovery. At low stimulation, the small nucleation probability causes a stochastic part of the ISI of considerable length, and the total ISI is the sum of the minimal ISI plus the stochastic part. The standard deviation caused by the stochastic part is often of the same order of magnitude as the total ISI (Figure 2) [26, 54, 55]. Taking additionally into account that successive ISIs are uncorrelated [26], we conclude that cellular concentration spike sequences generate random ISIs. The properties of the ISI probability distributions can be explained with the wave nucleation mechanism, which is simply the spatio-temporal manifestation of CICR.

How is this randomness compatible with the function of Ca^{2+} as a second messenger to transmit information? Encoding of the concentration of the extracellular agonist in the frequency of the Ca^{2+} spike sequences is one of the possible modes of information transmission [23, 30, 56-59]. The frequency increases with the agonist concentration. However, the stochastic character of the spike sequences causes a broad distribution of frequencies instead of a well-defined peak in the Fourier spectrum [55, 60]. Consequently, not only the average ISI (corresponding to frequency), but also other properties of the ISI distribution encode information. We used the Kullback Entropy to quantify information content (Figure 3). This measure is based on a reference process, as which we have chosen the spike sequence with constant spike probability, i.e., without feedback. The calculations showed that both negative and positive feedback lead to an increase in the maximal information content. Already the first measurements showed that the slope of the moment relation is cell type specific [26]. The slope of the moment relation of spontaneously spiking cells was measured to be 1. Hence, spontaneous spike sequences correspond to the reference sequence. The slope of cells spiking upon stimulation is smaller than 1 [26], in excellent agreement with the function of stimulated spiking to transmit information. The smaller the slope, the more pronounced is the maximum of the Fourier spectrum and the larger is the signal to noise ratio [60]. Positive feedback corresponds to a bursting mode of Ca^{2+} signaling and causes a slope of the moment relation larger than 1 (Figure 3) [55].

Biological pathways are always embedded in an environment largely determined by molecular fluctuations [61-65]. Signaling pathways on the scale of single cells can be tuned to high accuracy only

at very high costs in terms of energy consumption [66]. Therefore, apart from precise function, evolutionarily conserved biological systems also must be robust to noisy fluctuations [67-69]. Indeed, intracellular Ca^{2+} signals exhibit huge variability [70, 71]. Therefore, it can be expected that the Ca^{2+} signaling mechanism is not only specific, but also robust: Its biological function should not depend on high precision.

We found in theoretical investigations [36, 39] that the average ISI T_{av} depends sensitively on details like cluster size and cluster distance, which are different from cell to cell (Figure 4A). This is consistent with experiments showing huge cell-to-cell variability in T_{av} (see Figure 2). Obviously, the average ISI is not robust and consequently also not frequency encoding. How does Ca^{2+} signaling then robustly transmit information? That question has not been answered yet, but experiments and theoretical studies have offered first hints to robust properties.

The same experiments revealed that the relation between average and standard deviation is robust to cell-to-cell variability and contains information on the cell population (Figure 2). By mathematical modeling, we found that it is robust against changes of parameter values like puff probability, strength of spatial coupling, spatial cluster arrangement or channel closing rate, i.e. parameter values that distinguish individual cells of the same cell type (Figure 4B) [36, 39]. Importantly, we did not postulate any assumptions about robustness to cell-to-cell variability when formulating the model. In the contrary, we assumed the highest possible irregularity (Poisson statistics [72]) for the dynamics of the single clusters [39]. The most important ingredient of the model was strong coupling of IP_3R within a cluster, causing the IPI and puff duration distributions given in Equations 1-2, which were validated by live cell imaging [35, 50]. Thus, we found that highly stochastic molecular dynamics in combination with emergent behavior can result in robustness.

In the model simulations shown in Figure 4B, the slope of the moment relation is always one, but in many cell types, the slope is smaller than one (Figure 2C), which corresponds to a higher signal to noise ratio. How do cells improve the signal to noise ratio to values larger than one ? We found only one possibility – global negative feedback. In addition to the local feedback mechanisms resulting from the bell shaped Ca^{2+} response curve, Ca^{2+} signaling pathways also contain global feedbacks from a cellular spike onto the activity of the clusters. A typical example is Ca^{2+}-activated Protein kinase C, which inhibits G-protein coupled receptors. Including such global negative feedback into the model substantially reduced the slope of the relation between average and standard deviation of ISIs (Figure 4C) [39].

4. Modeling of stochastic Ca^{2+} signals

The choice of the mathematical framework depends on the purpose of the modeling study. Describing the complete spectrum of Ca^{2+} signals without *a priori* assumptions on the signal type requires multi-scale models or hierarchic stochastic models. Inclusion of Ca^{2+} spiking into models of complex pathways, which can dispense with detailed dependencies of spike duration on system parameters, can be achieved very easily by using ISI distributions.

Following the ideas of multi-scale models, we developed a novel simulation algorithm called the *Green's Cell* (GC). It combines the time and length scales depicted in Figure 1 [36, 60]. We describe a single channel by a Markov chain according to the DeYoung-Keizer model. Thus, the binding event of an IP_3 molecule or Ca^{2+} ion is explicitly determined by a hybrid version of a Gillespie algorithm in dependence on the local Ca^{2+} concentration. An open channel leads to a blip and might activate other channels in the cluster. The resulting local Ca^{2+} concentration is determined by a quasi-steady state approximation derived in ref. [51]. On the cell level, the concentration dynamics are governed by a spherical reaction-diffusion system, which describes free Ca^{2+} as well as a mobile and immobile Ca^{2+}

buffer using a multicomponent Green's function. The open clusters are the stochastic source terms in the Green-integral. The analytical solution of the reaction-diffusion system renders the simulations very efficient, since we only have to calculate the concentrations at cluster locations for possible channel transitions, whereas purely numerical solvers always have to update the concentration at each grid point throughout the whole volume.

The model is able to reproduce all experimentally known Ca^{2+} signals in dependence on physiological parameters including diffusion and buffer properties, cell radius and cluster arrangement as well as SERCA activity and IP_3R properties [36]. The mechanistic approach allows us to follow a Ca^{2+} spike from its triggering event, the stochastic opening of a first channel, all the way up to the cellular concentration spike as shown in Figure 1. Since we can control and monitor all dynamic processes in the model we can estimate the role of the different building blocks for the different signal forms. Figure 5A exhibits a representative time series obtained by GC simulation, which is in good agreement to experimental measurements. By varying parameters, the regular spiking can be tuned into more irregular and slower spiking or into a kind of plateau response with superimposed oscillations. In this way we produced a variety of different Ca^{2+} spiking signals and determined analogously to experiments the dependence of the standard deviation σ on the average period T_{av} of the resulting spike trains. This is shown in Figure 5B where again each dot corresponds to such a spike train of one *in silico* cell. Like in the experimental analysis, we observe an offset on the T_{av} axis that corresponds to the deterministic recovery period. The slope of this relation is close to 1 indicating spontaneous spiking (as seen in astrocytes) that obey the characteristics of a Poisson process with a regeneration period. Moreover, we could reproduce the experimentally observed effect that loading additional Ca^{2+} buffer renders spiking slower and more irregular.

In extensive simulations, we used fixed cellular setups and varied only one specific parameter leading to parameter specific moment relations. They exhibit the robustness properties described above. Variation of the spatial distance between channel clusters, the stimulation level in terms of the IP_3 concentration or the pump strength over one order of magnitude leads to a similar slope for a population of cells, which are distinguished by the mobile buffer concentration. For standard values with single channel fluxes of 0.12 pA, the slope was always close to 1 and therefore in the range of spontaneous oscillations as shown in Figure 5C.

The Green's cell method was used to study the effect of variations of molecular properties on cellular dynamics [9]. We found in patch clamp experiments that isolated channels have a mean open time of 10 ms whereas open times of single channels located in a channel cluster have a halved open time of 5 ms. Whether such a change on a ms time scale can influence the cell dynamics on a 100s-time scale is hard to answer in experiments, since information on the degree of clustering and channel behavior *in vivo* is difficult to obtain. We performed simulations of identical *in silico* cells with different IP_3R properties. We compared global Ca^{2+} signals from cells with only isolated channels with cells having the same number of channels arranged in clusters and obeying the different opening times. It turns out that clustering and the change on a microscopic time scale have major impacts on the global dynamics. For isolated and diffusively arranged channels no global Ca^{2+} spikes were observed in the physiological parameter range. Due to clustering of these channels, the cell exhibits Ca^{2+} spikes even with a halved open time. The corresponding cellular setups with a hypothetical doubled open time lead to more frequent spiking with a on average 4 times faster mean period.

The problem with detailed models is the limited knowledge of *in vivo* parameter values for channel state dynamics. But even if we knew them, formulation of a complete stochastic theory would be impossible due to state space explosion, since a single channel of the DeYoung-Keizer model has already 330 states, already. We developed the strategy of *hierarchic stochastic modeling* to circumvent both of these problems [39]. It exploits emergent behavior caused by the hierarchical structure of the

Ca^{2+} signaling machinery.

The cellular dynamics are determined by the distributions of puff amplitude, puff duration and IPI of the cell's puff sites. Hence, we can formulate a cell model directly in terms of these distributions and some information on cluster coupling (Figure 6) [39]. The distributions have been measured *in vivo* [12, 14, 33, 35, 73, 74]. Thus, the model uses experimental input data without requirement for information on many parameters of channel state dynamics [39]. Clusters are described by one closed state with an open time distribution (single site IPI distribution, see Equation 1) and an open state with a closing time distribution (puff duration distribution, see Equation 2). In a setup with N_c channels, the number of states is reduced from 330^{Nc} to 2. However, the price that we pay for this considerable reduction is that the master equation becomes a system of integro-differential equations instead of the original ordinary differential equations. The master equation formulation can be used to calculate ISI interval distributions and other characteristics [70,71]. The model can also be used for simulations [39].

With this probabilistic model, we are able to predict the relation (see Figure 4). The efficiency of the simulations with that model and partially analytical calculations were instrumental for the prediction of the robustness properties of the moment relation. We analyzed also the dependence of modes of behavior like spiking and bursting on system parameters [39].

The Green's cell model and the hierarchic stochastic model provide efficient frameworks to compute cellular Ca^{2+} spike sequences from cellular parameters. Both approaches are based on experimental findings and were validated by in vivo data. The hierarchic stochastic model, in particular, also can be implemented in an efficient way which should permit its integration into larger models describing signaling networks. Nevertheless, for practical applications it would be advantageous to define a stochastic process with few generic parameters, which correctly samples the stochastic part of ISI but does not consider details of the spike generating mechanism. Samples of this stochastic process would provide realistic spike sequences, which can be used in systems level investigations [75, 76] including Ca^{2+} signals. We found that it is indeed possible to follow such a generic modeling strategy, without neglecting important characteristics of the spike generating machinery.

A similar ansatz as chosen for the IPI distributions (see Equation 1) describes also the distributions *P(t)* of the stochastic part *t* of the ISI very well. We introduce an additional parameter λ_1, which is negative in case of negative feedback and positive for positive feedback:

$$P(t) = \lambda(1+\lambda_1 e^{-\xi t})\exp[-\int_0^t \lambda(1+\lambda_1 e^{-\xi t'})dt'] = \lambda(1+\lambda_1 e^{-\xi t}) e^{-\lambda t} \exp\left[-\frac{\lambda\lambda_1}{\xi}\left(1-e^{-\xi t}\right)\right]. \quad (3)$$

The cumulative distribution function $P_c(t)$ is

$$P_c(t) = \int_0^t P(t')dt' = 1-\exp\left[-\frac{\lambda\lambda_1}{\xi}\left(1-e^{-\xi t}\right)-\lambda t\right]. \quad (4)$$

A straightforward modeling strategy that suffices for many purposes is to draw *t* from the cumulative distribution and to set the sample ISI equal to $T_{min}+t$, with T_{min} being the minimal ISI. We found that experimental distributions with a slope of the moment relation between 0.5 and 1 are well described with the choice λ_1=-1 (see Figure 3).

Distributions with slopes of the moment relation smaller than 0.5 cannot be generated by Equation 4. The fact that some cell types (e.g. HEK cells) exhibit slopes in the range of 0.2 (see Figure 2) indicates more complex dynamics. This can be accounted for by considering cooperativity in the global feedback [77], which can be captured by

$$r(t) = \lambda(1 - e^{-\xi t})$$

$$P(t) = \lambda_2 \frac{r(t)^n}{K^n + r(t)^n} \exp[-\int_0^t \lambda_2 \frac{r(t')^n}{K^n + r(t')^n} dt'] \quad (5)$$

and the corresponding cumulative distribution function (Figure 7). The variable r(t) can be thought of as the concentration of a downstream factor mediating global negative feedback - it is temporarilly inhibited by cellular Ca^{2+} signals and regulates the open probability by cooperative binding. λ_2 would then be the maximal rate of spike initiation, n the Hill coefficient and K the half saturation constant. These kinetic parameters depend on the specific pathway that provides for the negative feedback. This form of the distribution can generate very small slopes down to 0.1 (Figure 7), and it correctly reproduces the statistics of all measured ISI sequences available so far.

The use of distributions for modeling purposes requires knowledge about dependences of distribution parameters on cellular parameters. First results for the parameter dependences of λ and ξ exist for the case λ_1=-1, n=0, λ_2=1 (i.e., for Equations 3-4): Changing the strength of spatial coupling by loading Ca^{2+} buffers into the cytosol changes only λ [36, 54], since it moves the cell along the moment relation in the SD-average plane, but does not change the relation. Theoretical investigations came to the same conclusion [39]. The value of ξ is equal to the time scale of recovery from global feedback, and T_{min} is equal to the smallest average ISI observed with the cell sample. These two parameters are cell type specific, while λ varies between individual cells and increases with increasing stimulation. The calculations in ref. [39] and the simulations in ref. [36] strongly suggest that λ in Equation 3 depends only on parameters the value of which distinguishes individual cells of the same cell type. However, a rigid mathematical proof is still lacking.

Mathematical modeling revealed a surprising reduction of complexity by the stochastic behavior. The stochastic scheme for the channel state dynamics has 11 parameters, the diffusion and buffering in the cytosol another 10 parameters, SERCAs, ER-cytosol volume ratio, single channel currents, luminal buffering, spatial cluster arrangement add even more parameters. Nevertheless, ISI distributions are in most cases described by only 3 parameters. The modes of behavior can also be identified by only two parameters, one parameter characterizing puff duration and the strength of spatial coupling [39]. The coupling is defined as the probability that a single open cluster opens a second one before it closes. Hence, all the tens of biological parameters describing the cell and molecules collapse onto 2 or 3 parameters that describe the spiking behavior. The robustness of the slope of the moment relation is related to this enormous reduction of complexity. If a subset of biological parameters determines only one specific parameter describing the distribution, the moment relation will not depend on this subset, i.e. it is robust against changes of the values of these parameters.

5. Conclusion

IP_3 induced Ca^{2+} release is organized hierarchically and each structural level (channel, channel cluster, cell) has its own dynamic characteristics. Puffs occur randomly and terminate within tens of milliseconds and interpuff intervals last a few seconds. Interaction between clusters via Ca^{2+} diffusion and CICR generates cellular Ca^{2+} spikes, which also occur randomly. The interspike interval (ISI) has a deterministic and a stochastic part. The deterministic part is the minimal ISI caused by recovery of the cell from the previous spike, and the stochastic part starts after sufficient recovery. The standard deviation of ISI is determined by the stochastic part. If the spike generation probability after recovery is very high at strong stimulation, the next spike will occur very soon after recovery and the spike sequences becomes almost regular. Puffs and spikes exhibit different time scales, since not every puff initiates a spike. The weaker the coupling of clusters by Ca^{2+} diffusion and CICR is, the smaller is the

probability that a puff sets off a spike (coupling probability). This causes the sensitive dependence of ISI on buffer concentration.

Average ISI vary strongly among cells, i.e. they are not robust against cell-to-cell variability. The moment relation between the standard deviation and the average of ISI is robust. It has a slope equal to 1 for spontaneously spiking cells and a slope smaller than 1 for cells spiking upon stimulation. Hence, stimulated spike sequences exhibit reduced randomness, which favors information transmission. A slope of the moment relation smaller than 1 indicates the existence of negative feedback, and a slope smaller than 0.5 indicates additional cooperativity in this feedback. Consequently, we can obtain information on cellular feedback mechanisms by the analysis of ISI statistics. A more detailed theoretical analysis of the effect of feedbacks on the moment relation and ISI statistics will most likely reveal more information that we can obtain from cellular measurements.

Another question deserving future theoretical and experimental investigation is how downstream parts of the Ca^{2+} signaling pathways deal with the randomness of spike sequences. Additionally, the lack of robustness of average ISI against cell variability points towards a missing universal correlation between extracellular agonist concentration and average ISI. Cells respond either with slow or with fast spiking to the same agonist concentration. How do downstream parts of the pathway correct for this variability in a cell specific manner, in order to conclude the correct value of the extracellular concentration from the Ca^{2+} spike sequence? Or, do they not correct for it? The results of these investigations will not only provide deeper understanding of Ca^{2+} signaling but also on cell signaling and the meaning of agonist concentration values in general.

As the signal-to-noise ratio of the Ca^{2+} signal is pathway specific, and some cells even use the signaling mode with least signal precision, the Ca^{2+} signaling mechanism does not seem to have evolved toward maximal signal quality. This questions the paradigm that noise suppression is a primary goal of the design of signal transduction pathways [64] or of biological systems in general [65]. The inherent robustness of the moment relation in the Ca^{2+} signal suggests that tight control of the noise level and possibly of noise statistics might be more beneficial than the highest possible precision.

The noise is beneficial for analysis of cell behavior. The standard deviation of ISIs contains information on the puff probability and nucleation probability *in vivo* and their dependence on experimental conditions. The moment relation between SD and average indicates the existence, time scales and cooperativity of feedbacks. Both properties are noise induced.

Acknowledgments

KT was supported by the Deutsche Forschungsgemeinschaft (SFB 555), an EMBO short-term fellowship and a Functdyn exchange grant of the European Science Foundation.

References

[1] M.J. Berridge, Inositol trisphosphate and calcium signalling, Nature, 361 (1993) 315-325.
[2] M.J. Berridge, M.D. Bootman, P. Lipp, Calcium--a life and death signal, Nature, 395 (1998) 645-648.
[3] M.J. Berridge, P. Lipp, M.D. Bootman, The versatility and universality of calcium signalling, Nat Rev Mol Cell Biol, 1 (2000) 11-21.
[4] C.W. Taylor, A.J. Laude, IP_3 receptors and their regulation by calmodulin and cytosolic Ca^{2+}, Cell Calcium, 32 (2002) 321-334.
[5] M. Falcke, Reading the patterns in living cells - the Physics of Ca^{2+} signaling, Advances in Physics, 53 (2004) 255-440.
[6] J.K. Foskett, C. White, K.-H. Cheung, D.-O.D. Mak, Inositol Trisphosphate Receptor Ca^{2+} Release Channels, Physiological Reviews, 87 (2007) 593-658.
[7] C.W. Taylor, P. Thorn, Calcium signalling: IP_3 rises again ... and again, Current biology : CB, 11 (2001) R352-R355.
[8] I.F. Smith, S.M. Wiltgen, I. Parker, Localization of puff sites adjacent to the plasma membrane: Functional and spatial characterization of Ca^{2+} signaling in SH-SY5Y cells utilizing membrane-permeant caged IP3, Cell Calcium, 45 (2009) 65-76.
[9] Taufiq-Ur-Rahman, A. Skupin, M. Falcke, C.W. Taylor, Clustering of $InsP_3$ receptors by $InsP_3$ retunes their regulation by $InsP_3$ and Ca^{2+}, Nature, 458 (2009) 655-659.
[10] W. Suhara, M. Kobayashi, H. Sagara, K. Hamada, T. Goto, I. Fujimoto, K. Torimitsu, K. Mikoshiba, Visualization of inositol 1,4,5-trisphosphate receptor by atomic force microscopy, Neuroscience Letters, 391 (2006) 102-107.
[11] M. Ferreri-Jacobia, D.O. Mak, J.K. Foskett, Translational mobility of the type 3 inositol 1,4,5-trisphosphate receptor Ca^{2+} release channel in endoplasmic reticulum membrane, J Biol Chem, 280 (2005) 3824-3831.
[12] M. Bootman, E. Niggli, M. Berridge, P. Lipp, Imaging the hierarchical Ca^{2+} signalling system in HeLa cells, The Journal of Physiology, 499 (Pt 2) (1997) 307-314.
[13] R. Thul, M. Falcke, Release currents of IP3 receptor channel clusters and concentration profiles, Biophys J, 86 (2004) 2660-2673.
[14] Y. Yao, J. Choi, I. Parker, Quantal puffs of intracellular Ca^{2+} evoked by inositol trisphosphate in Xenopus oocytes, The Journal of Physiology, 482 (1995) 533-553.
[15] J. Marchant, N. Callamaras, I. Parker, Initiation of IP(3)-mediated Ca(2+) waves in Xenopus oocytes, The EMBO Journal, 18 (1999) 5285-5299.
[16] M. Falcke, On the Role of Stochastic Channel Behavior in Intracellular Ca^{2+} Dynamics, Biophys J, 84 (2003) 42-56.
[17] R. Thul, M. Falcke, Stability of membrane bound reactions, Phys Rev Lett, 93 (2004) 188103.
[18] J.S. Marchant, I. Parker, Role of elementary Ca^{2+} puffs in generating repetitive Ca^{2+} oscillations, The EMBO Journal, 20 (2001) 65.
[19] R.E. Dolmetsch, K. Xu, R.S. Lewis, Calcium oscillations increase the efficiency and specificity of gene expression, Nature, 392 (1998) 933-936.
[20] W.-H. Li, J. Llopis, M. Whitney, G. Zlokarnik, R.Y. Tsien, Cell-permeant caged $InsP_3$ ester shows that Ca^{2+} spike frequency can optimize gene expression, Nature, 392 (1998) 936-941.
[21] H. Schulman, P.I. Hanson, T. Meyer, Decoding calcium signals by multifunctional CaM kinase, Cell Calcium, 13 (1992) 401-411.
[22] N.M. Woods, K.S. Cuthbertson, P.H. Cobbold, Repetitive transient rises in cytoplasmic free calcium in hormone-stimulated hepatocytes, Nature, 319 (1986) 600-602.
[23] T.A. Rooney, E.J. Sass, A.P. Thomas, Characterization of cytosolic calcium oscillations induced by

phenylephrine and vasopressin in single fura-2-loaded hepatocytes, J Biol Chem, 264 (1989) 17131-17141.
[24] G. Dupont, M.J. Berridge, A. Goldbeter, Latency correlates with period in a model for signal-induced Ca^{2+} oscillations based on Ca^{2+}-induced Ca^{2+} release, Cell Regul, 1 (1990) 853-861.
[25] M.J. Berridge, The AM and FM of calcium signalling, Nature, 386 (1997) 759-760.
[26] A. Skupin, H. Kettenmann, U. Winkler, M. Wartenberg, H. Sauer, S.C. Tovey, C.W. Taylor, M. Falcke, How does intracellular Ca^{2+} oscillate: by chance or by the clock?, Biophys J, 94 (2008) 2404-2411.
[27] G.W. De Young, J. Keizer, A single-pool inositol 1,4,5-trisphosphate-receptor-based model for agonist-stimulated oscillations in Ca^{2+} concentration, Proc Natl Acad Sci USA, 89 (1992) 9895-9899.
[28] J.P. Keener, J. Sneyd, Mathematical Physiology, Springer, New York, 1998.
[29] E. Gin, M. Falcke, L.E. Wagner, 2nd, D.I. Yule, J. Sneyd, A kinetic model of the inositol trisphosphate receptor based on single-channel data, Biophys J, 96 (2009) 4053-4062.
[30] S. Schuster, M. Marhl, T. Hofer, Modelling of simple and complex calcium oscillations. From single-cell responses to intercellular signalling, Eur J Biochem, 269 (2002) 1333-1355.
[31] J. Sneyd, M. Falcke, J.F. Dufour, C. Fox, A comparison of three models of the inositol trisphosphate receptor, Prog Biophys Mol Biol, 85 (2004) 121-140.
[32] l. Bezprozvanny, J. Watras, B.E. Ehrlich, Bell-shaped calcium-response curves of lns(l,4,5)P3- and calcium-gated channels from endoplasmic reticulum of cerebellum, Nature, 351 (1991) 751-754.
[33] I. Parker, J. Choi, Y. Yao, Elementary events of $InsP_3$-induced Ca^{2+} liberation in Xenopus oocytes: hot spots, puffs and blips, Cell Calcium, 20 (1996) 105-121.
[34] E.R. Higgins, H. Schmidle, M. Falcke, Waiting time distributions for clusters of IP_3 receptors, J Theor Biol, 259 (2009) 338-349.
[35] K. Thurley, I. Smith, S.C. Tovey, C.W. Taylor, I. Parker, M. Falcke, Time scales of IP_3-evoked Ca^{2+} spikes emerge from Ca^{2+} puffs only at the cellular level, Submitted, (2011).
[36] A. Skupin, H. Kettenmann, M. Falcke, Calcium Signals Driven by Single Channel Noise, PLoS Comput Biol, 6 (2010) e1000870.
[37] C.G. Schipke, A. Heidemann, A. Skupin, O. Peters, M. Falcke, H. Kettenmann, Temperature and nitric oxide control spontaneous calcium transients in astrocytes, Cell Calcium, 43 (2008) 285-295.
[38] M. Falcke, Buffers and Oscillations in Intracellular Ca^{2+} Dynamics, Biophys. J., 84 (2003) 28-41.
[39] K. Thurley, M. Falcke, Derivation of Ca^{2+} signals from puff properties reveals that pathway function is robust against cell variability but sensitive for control, Proc Nat Acad Sci USA, 108 (2011) 427-432.
[40] T. Meyer, L. Stryer, Molecular model for receptor-stimulated calcium spiking, Proc Nat Acad Sci USA, 85 (1988) 5051-5055.
[41] J. Sneyd, M. Falcke, Models of the inositol trisphosphate receptor, Prog Biophys Mol Biol, 89 (2005) 207-245.
[42] J.-L. Martiel, A. Goldbeter, A Model Based on Receptor Desensitization for Cyclic AMP Signaling in Dictyostelium Cells, Biophys J, 52 (1987) 807-828.
[43] G. Dupont, M.J. Berridge, A. Goldbeter, Signal-induced Ca^{2+} oscillations: properties of a model based on Ca^{2+}-induced Ca^{2+} release, Cell Calcium, 12 (1991) 73-85.
[44] J. Shuai, H.J. Rose, I. Parker, The number and spatial distribution of IP3 receptors underlying calcium puffs in Xenopus oocytes, Biophys J, 91 (2006) 4033-4044.
[45] G.W. De Young, J. Keizer, A single-pool inositol 1,4,5-trisphosphate-receptor-based model for agonist-stimulated oscillations in Ca^{2+} concentration, Proc Natl Acad Sci U S A, 89 (1992) 9895-9899.
[46] J. Ramos-Franco, S. Caenepeel, M. Fill, G. Mignery, Single channel function of recombinant type-1 inositol 1,4,5-trisphosphate receptor ligand binding domain splice variants, Biophys J, 75 (1998) 2783-2793.
[47] D.O. Mak, S. McBride, J.K. Foskett, ATP regulation of recombinant type 3 inositol 1,4,5-

trisphosphate receptor gating, J Gen Physiol, 117 (2001) 447-456.
[48] R. Thul, M. Falcke, Reactive clusters on a membrane, Phys Biol, 2 (2005) 51-59.
[49] D. Thomas, P. Lipp, S.C. Tovey, M.J. Berridge, W. Li, R.Y. Tsien, M.D. Bootman, Microscopic properties of elementary Ca^{2+} release sites in non-excitable cells, Curr Biol, 10 (1999) 8-15.
[50] I.F. Smith, I. Parker, Imaging the quantal substructure of single IP3R channel activity during Ca^{2+} puffs in intact mammalian cells, Proc Nat Acad Sci USA, 106 (2009) 6404-6409.
[51] K. Bentele, M. Falcke, Quasi-Steady Approximation for Ion Channel Currents, Biophys J, 93 (2007) 2597-2608.
[52] D. Fraiman, B. Pando, S. Dargan, I. Parker, S.P. Dawson, Analysis of puff dynamics in oocytes: interdependence of puff amplitude and interpuff interval, Biophys J, 90 (2006) 3897-3907.
[53] G. Dupont, S. Swillens, C. Clair, T. Tordjmann, L. Combettes, Hierarchical organization of calcium signals in hepatocytes: from experiments to models, Biochim Biophys Acta Mol Cell Res, 1498 (2000) 134-152.
[54] A. Skupin, M. Falcke, Statistical properties and information content of calcium oscillations, Genome Inform, 18 (2007) 44-53.
[55] A. Skupin, M. Falcke, Statistical analysis of calcium oscillations, Eur. Phys. J. Special Topics, 187 (2010) 231-240.
[56] N.M. Woods, K.S. Cuthbertson, P.H. Cobbold, Agonist-induced oscillations in cytoplasmic free calcium concentration in single rat hepatocytes, Cell Calcium, 8 (1987) 79-100.
[57] A. Goldbeter, G. Dupont, M.J. Berridge, Minimal model for signal-induced Ca^{2+} oscillations and for their frequency encoding through protein phosphorylation, Proc Nat Acad Sci USA, 87 (1990) 1461-1465.
[58] A.Z. Larsen, L.F. Olsen, U. Kummer, On the encoding and decoding of calcium signals in hepatocytes, Biophys Chem, 107 (2004) 83-99.
[59] M. Marhl, M. Perc, S. Schuster, A minimal model for decoding of time-limited Ca^{2+} oscillations, Biophys Chem, 120 (2006) 161-167.
[60] A. Skupin, M. Falcke, From puffs to global Ca^{2+} signals: How molecular properties shape global signals, Chaos, 19 (2009) 037111.
[61] M. Delbruck, The burst size distribution in the growth of bacterial viruses (bacteriophages), J Bacteriol, 50 (1945) 131-135.
[62] C.V. Rao, D.M. Wolf, A.P. Arkin, Control, exploitation and tolerance of intracellular noise, Nature, 420 (2002) 231-237.
[63] G. Balazsi, A. van Oudenaarden, J.J. Collins, Cellular decision making and biological noise: from microbes to mammals, Cell, 144 (2011) 910-925.
[64] N. Barkai, B.Z. Shilo, Variability and robustness in biomolecular systems, Mol Cell, 28 (2007) 755-760.
[65] A. Paldi, Stochastic gene expression during cell differentiation: order from disorder?, Cell Mol Life Sci, 60 (2003) 1775-1778.
[66] I. Lestas, G. Vinnicombe, J. Paulsson, Fundamental limits on the suppression of molecular fluctuations, Nature, 467 (2010) 174-178.
[67] H. Kitano, Biological robustness, Nat Rev Genet, 5 (2004) 826-837.
[68] J. Stelling, U. Sauer, Z. Szallasi, F.J. Doyle, 3rd, J. Doyle, Robustness of cellular functions, Cell, 118 (2004) 675-685.
[69] A. Wagner, Robustness and Evolvability in Living Systems, Princeton University Press, 2005.
[70] A. Skupin, H. Kettenmann, U. Winkler, M. Wartenberg, H. Sauer, S.C. Tovey, C.W. Taylor, M. Falcke, How does intracellular Ca^{2+} oscillate: by chance or by the clock?, Biophys. J., 94 (2008) 2404-2411.
[71] G. Dupont, A. Abou-Lovergne, L. Combettes, Stochastic aspects of oscillatory Ca^{2+} dynamics in hepatocytes, Biophys J, 95 (2008) 2193-2202.

[72] N.G. Van Kampen, Stochastic Processes in Physics and Chemistry, Elsevier Science B.V., Amsterdam, 2002.
[73] D. Thomas, P. Lipp, M.J. Berridge, M.D. Bootman, Hormone-evoked Elementary Ca^{2+} Signals Are Not Stereotypic, but Reflect Activation of Different Size Channel Clusters and Variable Recruitment of Channels within a Cluster, J Biol Chem, 273 (1998) 27130-27136.
[74] S.C. Tovey, P. de Smet, P. Lipp, D. Thomas, K.W. Young, L. Missiaen, H. De Smedt, J.B. Parys, M.J. Berridge, J. Thuring, A. Holmes, M.D. Bootman, Calcium puffs are generic InsP(3)-activated elementary calcium signals and are downregulated by prolonged hormonal stimulation to inhibit cellular calcium responses, J Cell Sci, 114 (2001) 3979-3989.
[75] H.V. Westerhoff, B.O. Palsson, The evolution of molecular biology into systems biology, Nat Biotechnol, 22 (2004) 1249-1252.
[76] H.V. Westerhoff, C. Winder, H. Messiha, E. Simeonidis, M. Adamczyk, M. Verma, F.J. Bruggeman, W. Dunn, Systems biology: the elements and principles of life, FEBS Lett, 583 (2009) 3882-3890.
[77] K. Wang, W.-J. Rappel, H. Levine, Cooperativity can reduce stochasticity in intracellular calcium dynamics, Phys Biol, 1 (2004) 27-40.

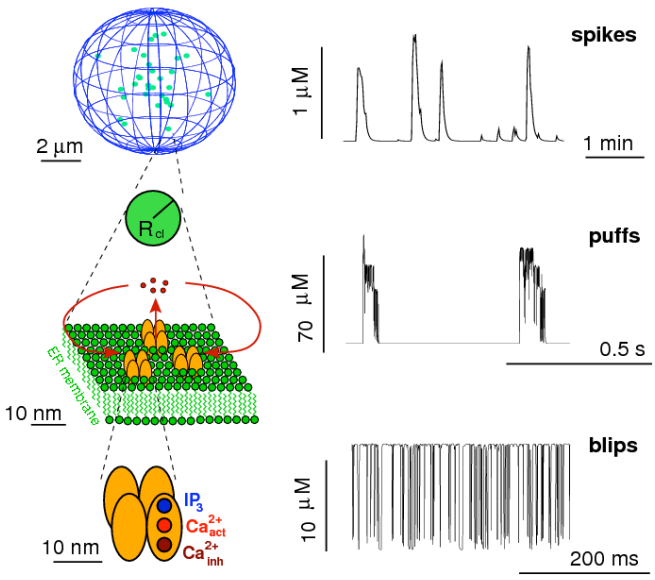

Figure 1: Mechanism of Ca^{2+} signaling. Hierarchical organization of the Ca^{2+} pathway with simulated signals of the corresponding structural level. The elementary building block of IP_3 induced Ca^{2+} signals is the IP_3R channel (bottom). It opens and closes stochastically. An open channel induces a Ca^{2+} influx into the cytosol by the large concentration difference between the ER and the cytosol. Since channels are clustered, opening of a single channel, which is called a blip, leads to activation of other channels in the cluster, i.e., a puff (middle). The cluster corresponds to a region with Ca^{2+} release with a radius R_{cl} that depends on the number of open channels. The stochastic local events are orchestrated by diffusion and CICR into cell wide Ca^{2+} waves, which correspond to spikes on the level of the cell (top).

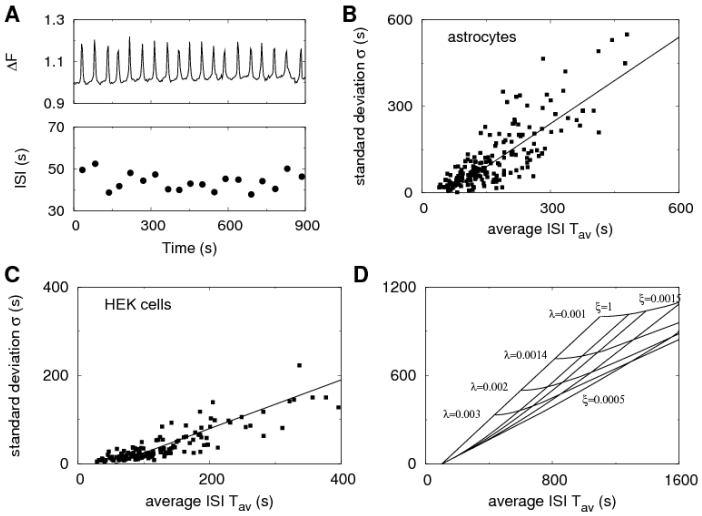

Figure 2: Ca^{2+} oscillations are stochastic. A: Representative time series of a single HEK cell stimulated by 30 μM CCh. The upper panel shows the fluorescent signal, which appears rather regular. By analyzing the individual interspike intervals (ISI) defined as the time between 2 fluorescent maxima, we see that also this apparently regular signal includes fluctuations. **B, C:** Dependence of standard deviation σ on the average ISI T_{av} of individual cells. The standard deviation depends linearly on the average ISI and is in the same range as the average for both spontaneous spiking astrocytes (B) and HEK cells stimulated with 30 μM CCh (C). This illustrates the stochastic nature of Ca^{2+} spiking. **D:** Theoretical prediction of the σ-T_{av} relation by the heuristic spiking model (Equations 3, 4) with λ_1=-1. The model includes spatial coupling and stimulation strength by the asymptotical nucleation rate λ and the recovery process by the regeneration rate ξ. From this model we see that stronger coupling and higher stimulation lead to faster spiking by large λ values. Furthermore, we observe that the slope of the relation depends on the regeneration rate ξ. For fast regeneration rates the slope is close to 1 (corresponding to a pure Poisson process). The slope decreases with decreasing ξ leading to more regular spiking. This illustrates how feedback mechanisms tune Ca^{2+} signals for different downstream targets. For more details see [26].

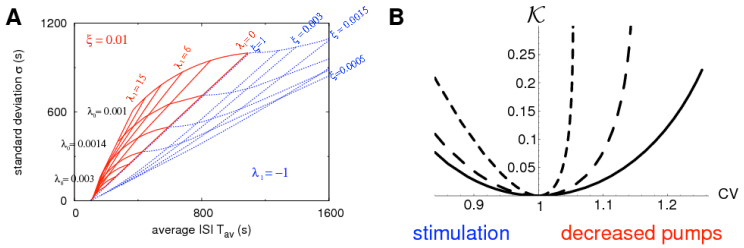

Figure 3: The moment relation reveals information content. A: Moment relation between the standard deviation σ and the average ISI T_{av} for negative (dashed blue) and positive (solid red) feedback (see Equations 3, 4). The offset on the T_{av}-axis correspond to a deterministic recovery period T_{min}. For $\lambda_1 = -1$ the slope decreases from 1 for $\xi \to \infty$ with decreasing ξ. The positive feedback leads to $\sigma > T_{av}$ for $\lambda_1 > 0$ and $\xi \neq \infty$. For $\lambda_1 > 0$, the σ-T_{av} relation exhibits a concave shape (all rates are given in s^{-1}). **B**: The information content measured by the Kullback entropy *K* in dependence on the CV= σ/T_{av} for $T_{min}=0$ and fixed $\lambda = 0.01\ s^{-1}$. Lines are generated by varying $\lambda_1 = -1 \ldots 1.5\ s^{-1}$ where negative values were observed in stimulated cells and positive λ_1 may arise due to small pump activity. ξ decreases from the bottom solid line to the upper line from $0.01\ s^{-1}$ to $0.005\ s^{-1}$ and to $0.002\ s^{-1}$. Figure from [55].

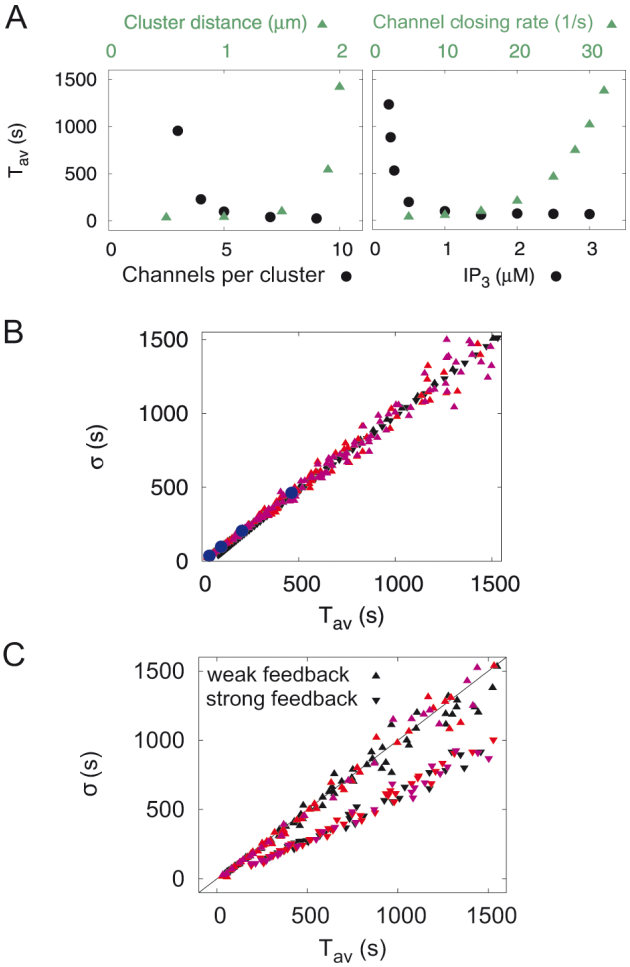

Figure 4: Ca^{2+} spikes are functionally robust. A: The average interspike interval T_{av} depends sensitively on cellular parameters. **B:** The slope of the relation of T_{av} and the standard deviation σ is equal to 1 for all values of parameters in the models without global feedback. Upper triangles: cluster distance a = 1.5 µm; lower triangles: a = 5 µm; black symbols: tetrahedron model; red symbols: regular cube model; pink symbols: cube model with randomly shifted vertex positions; blue circles: analytical solution of the tetrahedron model with a = 1.5 µm. **C:** The σ - T_{av} relation can be adapted by global feedback, implemented here by inhibition of the puff-rate after a global spike and recovery with rate ξ (Equation 1). All upper triangles: $\xi = 0.1\ s^{-1}$; all lower triangles: $\xi = 10^{-3}\ s^{-1}$. The relations are identical for the tetrahedron model (black symbols), the cube model (red) and the irregular cube model (pink). Reprinted from ref. [39].

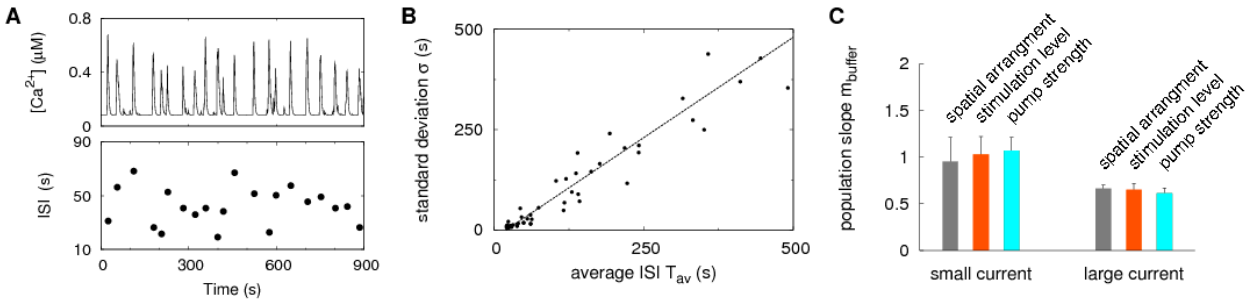

Figure 5: Modeling the Ca^{2+} signaling pathway by the Green's Cell algorithm. A: The simulated Ca^{2+} dynamics of a Green's cell exhibit a similar behavior as typical experimental time series. Analogously to Figure 2A, the upper panel shows the free cytosolic Ca^{2+} concentration and the lower panel the individual interspike intervals. **B:** The standard deviation – average ISI relation obtained from simulations. By varying IP_3, buffer and cytosolic calcium resting concentration, the Green's cell method produces a variety of different spike patterns from nearly regular oscillations to slow and random spiking. From the resulting spike trains, the standard deviation σ and the average period T_{av} were determined. Their linear relation has a slope close to 1 and thus corresponds to spontaneous spiking cells in experiments. The coincidence of this bottom-up approach with experiments indicates further that the puff-to-wave nucleation mechanism produces reliable relations between statistical quantities. **C:** Evidence for functional robustness. In extensive parameter scans, we analyzed the behavior of the σ-T_{av} relation. Interestingly, we found that the slope of the relation is rather robust against variations of the spatial cluster arrangement, IP_3 concentration and SERCA activity over one order of magnitude. For standard values leading to a single channel current of 0.12 pA the slope is always close to 1 whereas at ten times higher current of 1.2 pA leads to a slope of around 0.6 since concentration changes caused by individual clusters are not local anymore. For more details see [36].

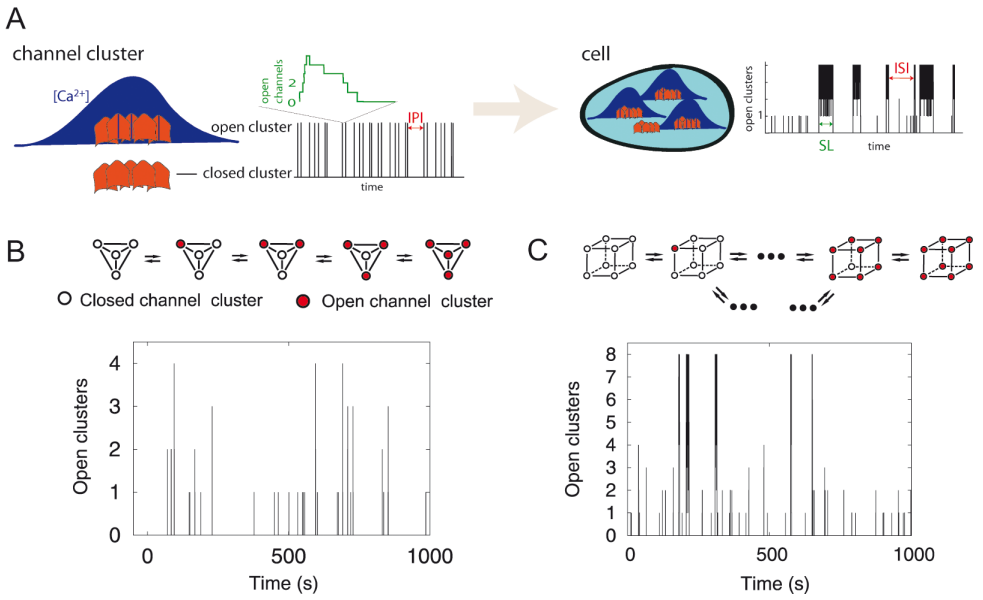

Figure 6: Hierarchic stochastic modeling of Ca^{2+} spikes. A: This recently developed modelling strategy starts from channel cluster characteristics. The interpuff interval IPI and puff duration distributions can be measured in vivo. That circumvents the problem arising from using parameter values of channel state dynamics from in vitro experiments for cell simulations. **B:** The model with 4 clusters arranged as the vertices of a tetrahedron is the simplest non-trivial implementation, because all configurations with the same number of open clusters are equivalent. Events with one open cluster correspond to puffs, and with 4 open clusters to spikes. **C:** The number of events with all clusters open (Ca^{2+} spikes) is similar to the tetrahedron model in the model with 8 clusters forming the vertices of a cube although the number of possible system configurations is much larger. Reprinted from main text and supporting information of ref. [39].

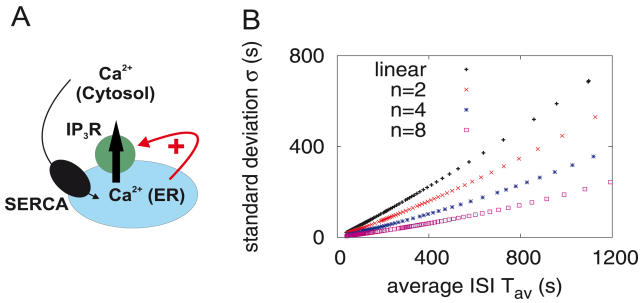

Figure 7: Cooperative feedback reduces the slope of the moment relation. A: We add cooperativity to the global feedback by considering Hill kinetics for an activator r(t) of Ca^{2+} channels, which is itself inhibited after a Ca^{2+} spike (Equation 5). **B:** Moment relations between average and standard deviation of interspike intervals resulting from cooperative feedback. The black + symbols are computed from Equation 3 with λ_1=-1 (i.e., linear response to r(t)), the other symbols result from Equation 5 with Hill coefficient n as indicated. Moment relations are obtained by variation of λ, other parameter values are λ_2=1, K=1 µM, ξ= 0.001 s^{-1}.